



Analysis of output power smoothing method of the solar chimney power generating system

Tingzhen Ming^{1,*†}, Fanlong Meng^{1,2}, Wei Liu¹, Yuan Pan³ and Renaud Kiesgen de Richter⁴

¹School of Energy and Power Engineering, Huazhong University of Science and Technology, No.1037, Luoyu Road, Wuhan, 430074, China

²College of Engineering, University of Arizona, 1130 North Mountain, P.O. Box 210119, Tucson, AZ 85721-0119, USA

³College of Electrical and Electronic Engineering, Huazhong University of Science and Technology, No.1037, Luoyu Road, Wuhan, 430074, China

⁴Tour-Solaire.Fr, 8 Impasse des Papillons, F34090 Montpellier, France

SUMMARY

Severe fluctuation of the output power is a common problem in the generating systems of various renewable energies. The concept of output power fluctuation factor of renewable energy power generating systems was put forward in this paper. Aiming to decrease the fluctuation factor of output power in solar chimney power generating systems (SC), a novel hybrid energy storage system made of water, and sandstone was employed to replace the traditional sandstone energy storage system. The mathematical models of fluid flow, heat transfer and power generating features of SC were established and the influences of material, depth, areas and location of the energy storage layer upon output power were analyzed. The simulation results indicated that adopting the hybrid energy storage of water and sandstone can effectively decrease the fluctuation factor of SC output power and hence smooth the SC output power. In addition, according to the largest daily power generating capability or the smallest peak fluctuation factor, the corresponding optimum depth of the water energy storage layer would be 5 cm or 20 cm, respectively. Copyright © 2012 John Wiley & Sons, Ltd.

KEY WORDS

solar chimney power generating system; fluctuation factor; output power; energy storage layer

Correspondence

*Tingzhen Ming, No.1037, Luoyu Road, Wuhan, China. School of Energy and Power Engineering, Huazhong University of Science and Technology, Wuhan, 430074, China.

†E-mail: tzming@mail.hust.edu.cn

Received 10 January 2012; Revised 3 September 2012; Accepted 8 October 2012

1. INTRODUCTION

The fluctuation and intermittence of wind energy and of solar energy have led to the same problems in output power of the existing wind power generation, solar photovoltaic and high-temperature thermal power generation, which are the shared features of renewable energy power generation nowadays. Experience has shown that serious output power fluctuation demands the large capacity of energy storage systems and power transmissions to network. This, however, may undermine the power generating grid connection aimed at commercial application. To smooth the fluctuation of renewable energy power generation systems, corresponding energy storage systems should be provided, which often cost a lot while storing little.

The solar chimney power generating system (SC) is a novel kind of renewable energy power generating system with continuous output power and relatively minor fluctuation. It is composed of four main parts: collector, energy storage

layer, turbine and chimney (as shown in Figure 1). The fundamental theory of this system has been described in detail in related publications written by the research group of Prof. Schlaich [1,2].

Since the construction of a 50kW SC prototype in Manzanares in Spain by Professor Schlaich's research group in 1982, many researchers have carried out related studies on the performance of this kind of system. Yan *et al.* [3] carried out systematical numerical simulation on fluid flow and heat transfer performances of SCs. Pasumarthi and Sherif [4,5], Padki and Sherif [6] also established mathematical models of fluid flow, heat transfer and output power features of the system and conducted comparative verification with the experimental results of their self-constructed power station. Considering the chimney friction coefficient and exit kinetic energy losses, Gannon and von Backström [7] made a thermodynamics cycle analysis based on a full-scale SC model, followed by another analysis considering the operating features of the

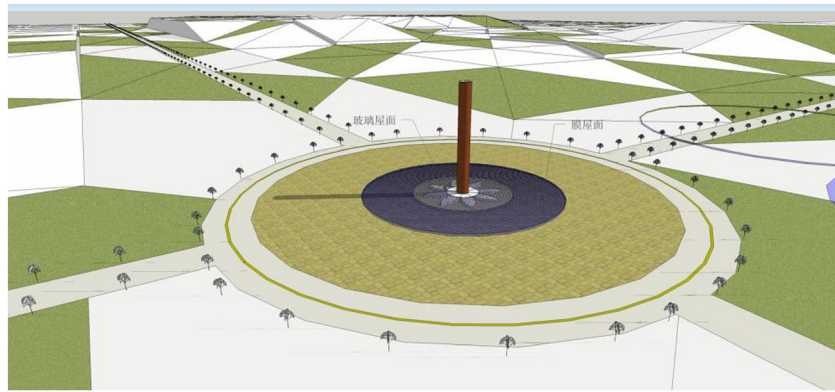


Figure 1. Schematic of solar chimney power generating system.

turbine and its influence on the system [8]. Bernardes *et al.* [9] developed mathematical models on heat transfer of systems with different collector structures and studied the influence of different factors upon output power. von Backström and Fluri [10] launched an analysis of the turbine pressure-drop coefficient corresponding to the highest output power. Pretorius and Kröger [11,12] carried out comprehensive system numerical simulation and analyses on the impact of different calculating methods on output power. Ming *et al.* [13] set up an analytical model of a system driving mechanism and carried out calculation to show the influence of system relative pressure and driving force on the output power and efficiency, followed by detailed study on thermodynamic cycle and unsteady fluid flow and thermal features of the SC system [14,15]. Bernardes *et al.* [16,17] made a comparative analysis between the results simulated by himself published in 2003 [9] and those by Pretorius [11] in the aspect of the influence of heat transfer coefficient upon the system output power, after which he looked into the effect of turbine pressure-drop coefficient on output power as well. More recently, Nizetic *et al.* [18] presented a detailed mathematical and cost analysis on the feasibility of implementing solar chimney power plants in the Mediterranean region. Maia *et al.* [19,20] and Ferreira *et al.* [21] gave detailed theoretical evaluations of the influence of geometric parameters and materials on the behavior of the airflow in an SC prototype and analyzed the airflow characteristics of the systems, which can also be used as driers for agricultural use. Nizetic and Klarin [22] presented a simplified analytical approach for evaluating the factor of turbine pressure drop in solar chimney power plants, in which it was concluded that for solar chimney power plants, turbine pressure-drop factors are in the range of 0.8–0.9. Ming *et al.* [23] presented an analysis on the influence of ambient crosswind on the thermal performance of SC. It is shown that the ambient crosswind has great negative influence on the output power of SC with ambient crosswind velocity is less than 15 m/s.

In addition, some researches also concentrated on shapes and configurations of the SC's chimney. In numerical calculation and theoretical analysis, Schlaich

et al. [24] chose the cylindrical chimney, with von Backström [10,24] and Pasumarthi *et al.* [4,5] using the divergent chimney and conical chimney, respectively. Based on constraints such as equal chimney bottom section area or equal chimney surface area, Ming *et al.* [25] analyzed the impact of several sizes of three different chimney configurations upon the chimney outlet air temperature and velocity, system output power and efficiency as well as the influence of the height to diameter ratio of the cylindrical chimney on system performance. However, the analysis of the chimney strength and resistance to wind load or to earthquakes, are also conducted by some researchers. The use of a double curvature surface is known for structure strengthening and quite often the cooling towers have hyperbolic shells and chimneys are usually reinforced by stiffening rings [26–28].

Apart from these studies, a lot of other researchers have carried out studies concerning the continuity and fluctuation of system output power. Kreetz *et al.* [29] performed numerical simulation on the system incorporating water energy storage, taking the Manzanares prototype as an example. Bernardes *et al.* [9] presented some simulation results of the influence exerted by the application of water energy storage layer on output power. Pretorius *et al.* [11] studied the effect of different types of materials upon output power. Ming *et al.* [30] and Xu *et al.* [31] conducted numerical simulation on the influence of energy storage layer on the power generating continuity. The results of Pretorius *et al.* [11] show that in terms of a typical SC of 100 MW that chooses sandstone as its major material, the ratio between peak and valley of output power within a day exceeds 6, which is still unacceptably high.

For SC systems whose output power should be sent to the power transmission network, it is vital to decrease the ratio between peak and valley of output power into a favorable scope. Thereby, the authors of this paper plan to find a way to solve this problem. As mentioned above, the SC with sandstone energy storage layer still has large fluctuation of output power, a novel hybrid energy storage layer made of water and sandstone will be

adopted to smooth the SC output power. Based on the SC models presented by Pretorius *et al.* [11] and Bernardes *et al.* [9], the mathematical models of SC with hybrid energy storage will be developed and the analysis of the impact of the materials, depth, areas and location of the energy storage layer on output power will be presented.

2. PHYSICAL AND MATHEMATICAL MODEL

2.1. Physical model

The basic dimensions and parameters of a 100 MW SC studied in this paper are shown in Table I. The sandstone is solely adopted in the energy storage layer while the hybrid energy storage layer employs both water and sandstone as demonstrated in Figure 2. We may dig an annular pool with a certain depth in the ground inside the collector, place a plastic bottom layer in case of water leaking and cover the water pool with a transparent film so as to create favorable conditions for solar energy absorption and evaporation prevention. During the process of numerical simulation, the plastic film on the water surface is assumed to be zero thickness and totally transparent to solar

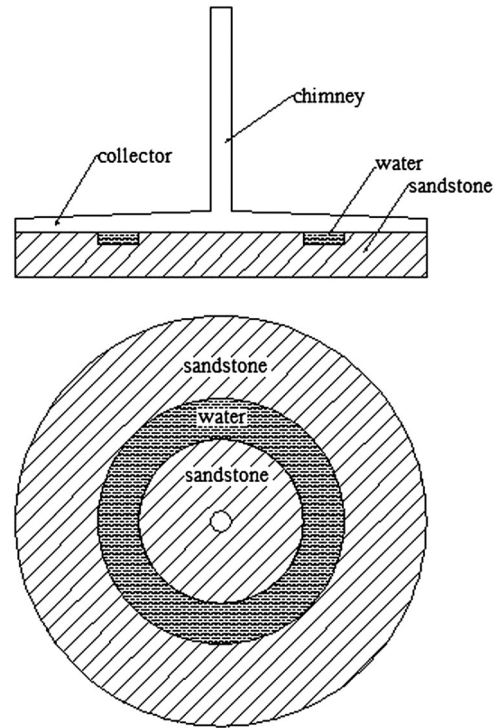


Figure 2. Schematic of SC system with hybrid energy storage.

Table I. Basic parameters of a 100 MW solar chimney power generation system [11].

Collector roof (glass)	
Emissivity of glass	$\epsilon_r = 0.87$
Roof shape exponent	$b = 1$
Perimeter (inlet) height	$H_l = 5 \text{ m}$
Outer diameter	$d_o = 5000 \text{ m}$
Ground	
Type	sandstone
Emissivity (treated surface)	$\epsilon_g = 0.9$
Absorptivity (treated surface)	$\beta_g = 0.9$
Density	$\rho_g = 2160 \text{ kg} \cdot \text{m}^{-3}$
Specific heat	$c_{pg} = 710 \text{ J} \cdot \text{kg}^{-1} \text{K}^{-1}$
Thermal conductivity	$\lambda_g = 1.83 \text{ W} \cdot \text{m}^{-1} \text{K}^{-1}$
Thickness	$Y_g = 5 \text{ m}$
Water	
Emissivity (treated surface)	$\epsilon_w = 0.9$
Absorptivity (treated surface)	$\beta_w = 0.4$
Extinction coefficient	$\alpha_w = 0.5$
Density	$\rho_w = 995 \text{ kg} \cdot \text{m}^{-3}$
Specific heat	$c_{pw} = 4174 \text{ J} \cdot \text{kg}^{-1} \text{K}^{-1}$
Thermal conductivity	$\lambda_w = 0.63 \text{ W} \cdot \text{m}^{-1} \text{K}^{-1}$
Chimney	
Height	$H_c = 1000 \text{ m}$
Inside diameter	$d_c = 210 \text{ m}$
Inner diameter	$d_i = 189 \text{ m}$
Turbine	
Turbo-generator efficiency	$\eta_g = 80 \%$
Inlet loss coefficient	$\eta_{turb,i} = 14 \%$
Ambient conditions	
Atmospheric pressure	$p_a = 90,000 \text{ N} \cdot \text{m}^{-2}$

radiation. Compared to the water tubes, the plastic film is much cheaper.

2.2. Mathematical model

The system performance of a solar chimney depends on the system dimensions and the ambient conditions. The former mainly includes the chimney height and radius and collector radius, while the latter includes the solar radiation, ambient temperature and wind velocity. The analysis described in this paper is based on the following simplifying assumptions:

- Axisymmetric flow of the air in the collector, i.e. non-uniform heating of the collector surface in terms of the sun's altitude angle is neglected. This assumption can simplify the numerical simulation procedure without causing large error to the results by three-dimensional numerical simulation results.
- Air flow inside the collector and the chimney can be regarded as incompressible flow, because the variations of both air velocity and pressure inside the system are not notable, and the air density changes slightly in the whole system.
- The collector is a slope from the inlet to the center of the collector canopy, which allows to keep a constant air volume and constant air speed before the air reaches the chimney.
- An average value for the optical properties of a certain material is used to estimate the solar radiation incident on the absorber surface. The transmittance of beam radiation during early sunshine hours would be

considerably lower than the average value of the transmittance which could lead to overestimation of the results.

(1) **Collector**

We divide the collector into several concentric sections of equal length along the radius direction, assuming a linear change of air temperature within every section and the exit temperature of the previous section being equal to the entrance temperature of the following, thus the exit temperature of the collector could be obtained by an iterative calculation from the inlet to the outlet of the collector along the radius direction. The continuity equation of the air within every section, air flow inside the collector being assumed to be incompressible flow, could be shown as follows:

$$\frac{\partial}{\partial r}(\rho_f u_f r H_{coll}) = 0 \tag{1}$$

In order to decrease the flow resistance, the collector can be designed as a slope increasing from its inlet to the outlet. Thereby, the change of the collector height according to the radius variation would follow [11]:

$$H_{coll} = H_{coll,i} \cdot \frac{r}{r_{coll,i}} \tag{2}$$

herein, $H_{coll,i}$ and $r_{coll,i}$ are the collector height at its inlet and the collector radius, respectively.

Within each section, the energy equations of collector canopy and air inside the collector are presented as follows:

$$h_{ra}(T_a - T_r) + h_{rf}(T_f - T_r) + h_r(T_g - T_r) = 0 \tag{3}$$

$$h_{gf}(T_g - T_f) + h_{rf}(T_r - T_f) = \frac{\dot{m}_f c_{pf}(T_{f,o} - T_{f,i})}{\pi \cdot r \cdot L} \tag{4}$$

where, T_a , T_r and T_g are the temperature of the ambience, the temperature of the canopy and the surface temperature of the absorber, respectively. $T_{f,o}$ and $T_{f,i}$ are the collector outlet and inlet air temperatures, respectively.

h_{ra} is the heat transfer coefficient between collector canopy and the ambient air which could be obtained [31]:

$$h_{ra} = 5.7 + 3.8u_a \tag{5}$$

h_r is the heat transfer coefficient by thermal radiation between the collector canopy and the energy storage layer surface, which could be seen as two relatively parallel planes:

$$h_r = \frac{\sigma(T_r^2 + T_g^2)(T_r + T_g)}{(1/\epsilon_r) + (1/\epsilon_g) - 1} \tag{6}$$

where, ϵ_r and ϵ_g are the emissivity of the collector canopy and energy storage layer surface, respectively.

h_{gf} , h_{rf} are the heat transfer coefficient by convection between the air and the collector canopy as well as the air and the energy storage layer surface, respectively. They could be obtained by equations (7)–(9), neglecting the influence of the roughness of the ground surface and the collector canopy [9].

$$\begin{cases} Nu = \frac{1}{\sqrt{\pi}} \sqrt{Re_x} \frac{Pr}{(1 + 1.7Pr^{1/4} + 21.36Pr)^{1/6}}, & Re < 5 \times 10^5 \\ Nu_{lam} = 2Nu_x \end{cases} \tag{7}$$

$$Nu = \frac{0.037Re^{0.8}Pr}{1 + 2.443Re^{-0.1}(Pr^{2/3} - 1)}, \quad 5 \times 10^5 < Re < 10^7, \quad 0.6 < Pr < 2000 \tag{8}$$

$$Nu = \sqrt{Nu_{lam}^2 + Nu_{tur}^2} \tag{9}$$

Similarly, the energy storage layer is divided into several sections from the ground surface to the bottom. Solar radiation is absorbed by the ground surface of energy storage layer, and the ground surface will transfer heat upward to the canopy by radiation, to the airflow inside the collector by convection and downward to the first section of the energy storage layer by conduction. Thereby, energy equations of the ground surface can be written as follows:

$$S + h_{gf}(T_f - T_g) + h_r(T_r - T_g) + \frac{\lambda}{0.5dz}(T_s - T_g) = 0 \tag{10}$$

where, $T_{s,1}$ is the temperature of the first section of the absorber, the distance between $T_{s,1}$ and T_g is 0.5 dz. As for the sandstone surface, $\lambda = \lambda_g$, and water surface, $\lambda = \lambda_w$, λ_g and λ_w stand for thermal conductivity of sandstone and water, respectively. S is the solar radiation energy absorbed by the surface of energy storage layer.

$$S = \beta \cdot S_{sun} \tag{11}$$

As to the sandstone surface, $\beta = A_E$, and the water surface $\beta = \beta_w, A_E$ and β_w stand for surface absorptivity of sandstone and water, respectively.

(2) **Energy storage**

The energy equation inside the energy storage layer is:

$$\rho c \frac{\partial T}{\partial \tau} = \frac{1}{r} \frac{\partial}{\partial r} \left(\lambda r \frac{\partial T}{\partial r} \right) + \frac{\partial}{\partial z} \left(\lambda \frac{\partial T}{\partial z} \right) + \dot{Q} \tag{12}$$

where, ρ and c are the density and specific heat at constant pressure of the energy storage layer, respectively. For the sandstone energy storage layer, solar radiation is absorbed in the first sub-layer and can be regarded as heat source: $\dot{Q} = \frac{S_{sun}}{\Delta z}$. From the second sub-layer to the bottom, no solar

radiation is absorbed: $\dot{Q} = 0$. For the water energy storage layer, solar radiation will penetrate and heat the water layer along its insolation path. Hence, in each sub-layer of the water energy storage layer, we can obtain the heat source as [32]: $\dot{Q} = \frac{S_{sun} \alpha_w (1 - \beta_w) e^{-\alpha_w z}}{\Delta z}$. While for the sub-layer of the sandstone energy storage under the water: $\dot{Q} = \frac{S_{sun} (1 - \beta_w) e^{-\alpha_w z}}{\Delta z}$.

The external and internal edges of the energy storage layer along the direction of depth were considered to be insulated:

$$\left. \frac{\partial T}{\partial r} \right|_{r=0} = 0 \text{ and } \left. \frac{\partial T}{\partial r} \right|_{r=R} = 0 \tag{13}$$

In the calculation, the bottom temperature of the sandstone energy storage layer located deep enough is viewed as constant.

(3) Chimney

Air flow inside the chimney can be regarded as an adiabatic expansion process when chimney wall heat losses are neglected. The variation rules of the parameters of air outside and inside the chimney based on the chimney height are essential for the system performance. The air density inside the chimney should be observed [9]:

$$\rho_c(z) = \rho_c(0) \left(1 - \frac{k-1}{k} \frac{z}{H_0} \right)^{1/k-1} \tag{14}$$

where, $H_0 = \frac{R_i T_{c,i}}{g}$, $T_{c,i}$ is the entrance air temperature; k is considered as 1.4005 [9,33].

The variation of air density outside the chimney according to height change observed:

$$\rho_a(z) = \rho_a(0) \left(1 - \frac{k-1}{k} \frac{z}{H_0} \right)^{1/k-1} \tag{15}$$

where, $H_0 = \frac{R_i T_a(0)}{g}$; $T_a(0)$ is the entrance air temperature and k is 1.235 considering the standard atmosphere [9,34].

(4) Turbine and power generator

The driving force that causes air to flow through the solar chimney power plant is due to a pressure difference between a column of cold air outside and a column of hot air inside the chimney, which provides the force to overcome the resistance of air flow and the pressure drop across the turbine:

$$\Delta p_{tot} = \Delta p_{dyn} + \Delta p_c + \Delta p_{c,i} + \Delta p_{coll} + \Delta p_{coll,i} + \Delta p_{turb} \tag{16}$$

The air exiting the chimney outlet experiences a loss in kinetic energy. This results in a dynamic pressure drop and is expressed as:

$$\Delta p_{dyn} = \frac{\rho_{c,o} \cdot u_{c,o}^2}{2} \tag{17}$$

The accelerating axial chimney airflow as well as the inside chimney wall friction both contribute to a pressure drop over the height of the chimney. The pressure drop in one section of the chimney is Δp_c .

$$\Delta p_c = k_c \cdot \frac{H}{d} \cdot \frac{\rho u^2}{2} \tag{18}$$

where, k_c is loss coefficient along the chimney [33]:

$$k_c = 0.11 \left(\frac{\Delta}{d} + \frac{68}{Re} \right)^{0.25} \tag{19}$$

herein, Δ is the roughness of the chimney, d is the chimney diameter.

The pressure drop over the chimney inlet is expressed in terms of a chimney inlet loss coefficient $k_{c,i}$ as [11]:

$$\Delta p_{c,i} = k_{c,i} \frac{\rho_{c,i} \cdot u_{c,i}^2}{2} \tag{20}$$

The pressure drop in the collector, Δp_{coll} , caused by accelerating radial airflow, roof and ground friction are all incorporated in:

$$\Delta p_{coll} = k_{coll} \cdot \frac{R}{d_{coll}} \cdot \frac{\rho u^2}{2} \tag{21}$$

where, k_{coll} is loss coefficient along the collector [35].

$$k_{coll} = \frac{54}{Re} \tag{22}$$

herein, R , and d_{coll} are the collector radius and collector hydrodynamic diameter, respectively.

The collector inlet pressure drop is [11]:

$$\Delta p_{coll,i} = (K_i + 1) \frac{\rho_a \cdot u_{coll,i}^2}{2} \tag{23}$$

where K_i is the collector inlet loss coefficient.

The turbine pressure drop is jointly determined by system draft power, the coefficient of turbine inlet losses as well as head loss of air flow within the system. The pressure-drop coefficient x is defined as the ratio between the pressure drop and system draft power and is considered as 0.85 in calculation:

$$x = \frac{\Delta p_{tot} - \Delta p_{loss}}{\Delta p_{tot}} \tag{24}$$

where, Δp_{tot} and Δp_{loss} can be written as follows:

$$\Delta p_{tot} = \int_0^H (\rho_0 - \rho_c) g dz \quad (25)$$

$$\begin{aligned} \Delta p_{loss} &= \Delta p_{dyn} + \Delta p_c + \Delta p_{c,i} + \Delta p_{coll} + \Delta p_{coll,i} \\ &= \zeta_{loss} \cdot \frac{\rho u^2}{2} \end{aligned} \quad (26)$$

The velocity of chimney inlet could be obtained according to system momentum equation [9].

$$u = \sqrt{\frac{2}{\rho} [(1-x)\Delta p_{tot} - \Delta p_{loss}]} \quad (27)$$

By combining equations (24), (26) and (27), we get:

$$u = \sqrt{\frac{2}{\zeta_{loss}\rho} (\Delta p_{tot} - \Delta p_{turb})} = \sqrt{\frac{2}{\zeta_{loss}\rho} (1-x)\Delta p_{tot}} \quad (28)$$

The SC turbine is pressure-based whose shaft output power can be obtained as follows:

$$P = x\Delta p_{tot} \frac{\dot{m}_f}{\rho} \quad (29)$$

The relation between the electric output power and turbine shaft output power is:

$$P_{elec} = \eta_g P \quad (30)$$

where, η_g is the power generating efficiency.

(5) Fluctuation factor

As stated before, the fluctuation and intermittence of renewable energies lead to fluctuating and intermittent output power, which bring difficulties for grid connection. Thereby, we should take into consideration their stability and continuity when evaluating the performances of renewable energy power generating systems. Here, the fluctuation factor of electric output power is defined as the ratio between the output power of the system at different times of the day and the minimum output power, that is:

$$F_{elec} = \frac{P_{elec}}{P_{elec, \min}} \quad (31)$$

where, F_{elec} is the fluctuation factor; $P_{elec, \min}$ is the minimum output power within a day. Obviously, along with the increase of the minimum $P_{elec, \min}$, the maximum $F_{elec, \max}$ will decrease and the fluctuation factor F_{elec} curve will become flatter, which leads to a more stable system output power. In reverse, the decrease of fluctuation factor minimum will result in a bigger maximum $F_{elec, \max}$ and a steeper fluctuation factor curve F_{elec} , thus leads to more unstable system output power.

If the fluctuation factor minimum $P_{elec, \min}$ is zero and appears sporadically within a day, the system output power will be intermittent.

3. CALCULATING METHOD

The material physical parameters, structure sizes, environment parameters, and the starting time, initial temperature of the energy storage layer as well as initial air velocity at the collector inlet should be given before numerical calculation which was performed in the software MATLAB R2009a. The air temperature and velocity of each section can be obtained by iterative calculation. Based on the air velocity and temperature, temperature of the energy storage layer, flow resistance, system draft power, output power as well as other essential parameters could be obtained. The calculation will not end in the present time step and enter the next time step until the residual results of all parameters ($\frac{\varphi_{N+1} - \varphi_N}{\varphi_N}$) between consecutive iterative calculations are within the 10^{-6} . The temperature and velocity distributions of the system of the previous time step will serve as the initial temperature and velocity distributions of the next time step. Such circulation would not stop until the last time step. The time step is 300 s, and there are 400 subsections along the radius inside the collector. In the energy storage layer, large temperature gradient will occur in about 0.1 m depth under the ground, so 30 subsections are assigned to this depth, also 30 other subsections are assigned to the remaining 4.9 m deeper under the ground. Simulations by using MATLAB R2009a indicated that further increasing the subsections of the system will not change the simulation results, so the numerical simulation results can be regarded as grid independent. The measured results in this paper all come from that of the 30th day to remove the negative influence caused by initial conditions of temperature, velocity, output power of the system and other parameters.

4. VERIFICATION AND COMPARISON WITH EXISTING RESULTS

To verify the reliability of the mathematical model in the paper, the parameters, such as ambient air temperature, solar radiation and ambient speed, all come from the data in reference [11] shown in Table II, and the bottom temperature of the energy storage layer is 313.5 K.

It can be seen from Figure 3 that simulation results in this paper and that presented by Pretorius [11] are pretty similar to each other, for they are nearly the same in peak value and the peak-to-valley occurrence time, with less than 4 MW difference in valley value. The disparity between them could be attributed to several reasons such as different selection of heat transfer coefficients, flow resistance model of the system, turbine pressure-drop coefficient and ignoring the influence of ambient relative

Table II. Solar radiation and environment temperature used in calculation [11].

Time	1	2	3	4	5	6	7	8
Solar radiation [$\text{W}\cdot\text{m}^{-2}$]	0	0	0	0	0	157	375	587
Ambient temperature [$^{\circ}\text{C}$]	24.92	24.49	24.06	23.63	23.20	22.77	22.34	21.91
Wind speed (m/s)	2.69	2.67	2.59	2.72	2.83	2.82	3.04	3.53
Time	9	10	11	12	13	14	15	16
Solar radiation [$\text{W}\cdot\text{m}^{-2}$]	773	917	1009	1040	1009	917	773	587
Ambient temperature [$^{\circ}\text{C}$]	24.00	25.80	27.40	28.60	29.70	30.10	30.40	30.30
Wind speed (m/s)	4.01	4.27	4.33	4.39	4.44	4.38	4.22	4.11
Time	17	18	19	20	21	22	23	24
Solar radiation [$\text{W}\cdot\text{m}^{-2}$]	375	157	0	0	0	0	0	0
Ambient temperature [$^{\circ}\text{C}$]	29.70	28.90	27.50	27.07	26.64	26.21	25.78	25.35
Wind speed (m/s)	4.06	4.01	3.63	3.19	3.27	3.13	2.92	2.78

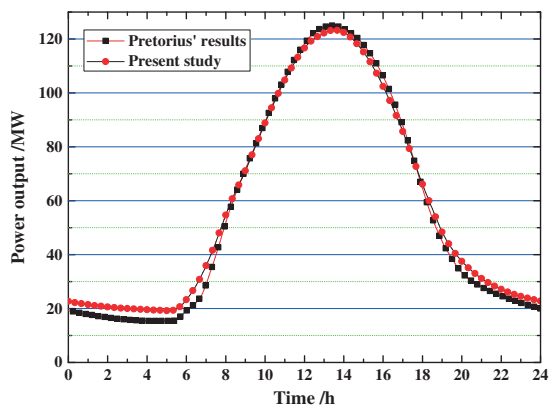


Figure 3. Comparison between present study and Pretorius' results [11].

humidity. Besides, the horizontal thermal transfer inside the energy storage layer has been taken into consideration while developing the mathematical model in this paper. To conclude, the calculating model proposed in this paper is validated as it is comparable to published literature.

5. RESULTS AND ANALYSIS

5.1. Influence of energy storage materials on SC performances

Solar radiation could be transmitted to energy storage on a medium surface in the daytime through the collector canopy; the radiation absorbed would raise the energy storage temperature. During the day, a fraction of the thermal energy of the energy storage layer will be transferred to the air flow inside the collector by convection, with the rest being stored by the energy storage layer and a small part transferred to the deeper ground (sand layer). At night, due to unavailability of solar radiation, the energy storage layer will continuously deliver back the energy stored during the daytime to the air inside the collector providing a

stable air flow, thus driving the turbine to deliver output power steadily. It is obvious that the total output power, i.e. the power generating capacity, at night is directly related to the amount of thermal energy provided by the energy storage layer to the air flow, thus the energy storage features of the materials would exert a great impact on the characteristics of the SC system's round-the-clock output power.

Figure 4 shows the influence of energy storage materials on the system output power within a day. Herein, $D_w = 10\text{ cm}$ represents the hybrid energy storage system of water and sandstone in which the water occupies a 10 cm depth on the energy storage layer with sandstone being placed below, while $D_w = 0\text{ cm}$ means only sandstone is used. It can be seen from this figure that, comparing with sole sandstone energy storage, adopting the hybrid energy storage of water and sandstone would notably narrow the output power peak-valley difference within a day. The output power peak value of the former system is 123.29 MW, while that of the latter is about 85.12 MW, namely 38.2 MW lower. Moreover, the hybrid system, whose output power minimum is 40.29 MW, with 21 MW higher than the sandstone one (19.19 MW), has greatly enhanced the system generating capacity at night when there is no solar radiation. The

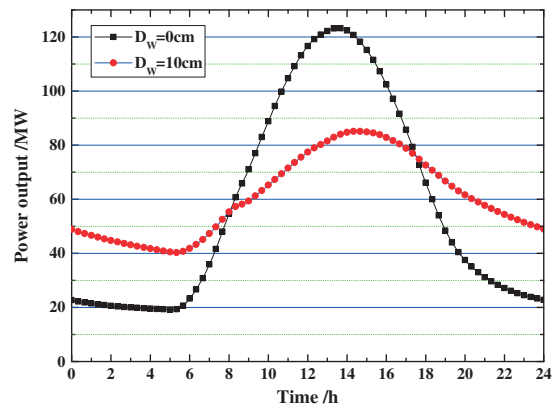


Figure 4. The influence of energy storage materials upon output power.

simulation results also indicate that, when comparing with the sole sandstone energy storage, the hybrid one would increase the total generating capability within a day due to heat absorption disparity between the two surfaces. The sandstone surface absorbs most of the solar radiation with the residual being reflected, while as for the water energy storage surface, around 40% of the radiation is absorbed by water and some of it serves to heat the whole water energy storage layer, with the residual completely being used for sandstone surface heating. It follows that, during the day, the hybrid energy storage system stores more energy than the sandstone one and transmits less to the air inside the collector, thus resulting in lower power generating capability during daytime. At night, reversely, the former one provides more energy to the air, to generate more power.

Figure 5 demonstrates the variation curves of the fluctuation factor within a day under two different energy storage systems. The maximum value of fluctuation factor of the sandstone system is 6.42, while that of the hybrid one is only 2.11, which has been notably decreased. It follows that the hybrid system is able to greatly narrow the fluctuation range of system output power, and helps in building a stable SC.

5.2. Influence of water layer depth on SC performances

The impact of the depth of water layer upon SC output power performances will be analyzed by adopting the hybrid energy storage system of water and sandstone in which water and the collector are equal in area, that is, water covers the whole surface of the energy storage layer. The depth of water layer is considered as 5 cm, 10 cm, 15 cm, 20 cm, 30 cm, 40 cm and 50 cm, respectively, in the computation. Figures 6, 7 and Table III show the influence of the water layer depth under the seven circumstances mentioned above, on the system performances, such as the output power and fluctuation factor. In the daytime, the decrease in the energy transmitted from the energy storage surface to the air flow, caused by the increase in water layer depth, leads to a lower output

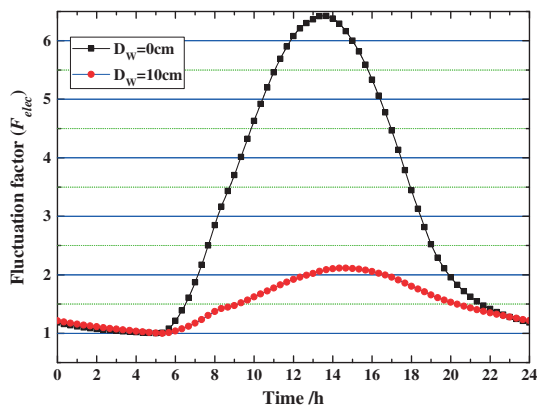


Figure 5. The influence of energy storage materials upon system fluctuation factor.

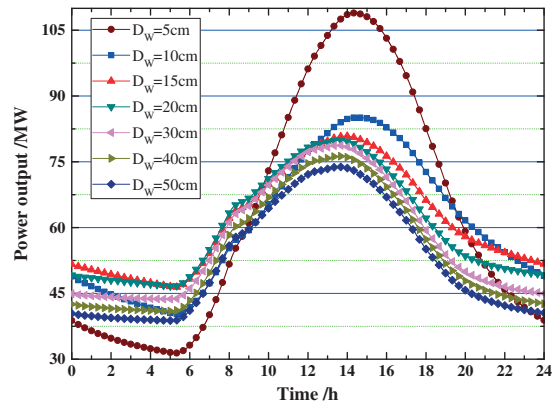


Figure 6. The influence of water layer depth on system output power.

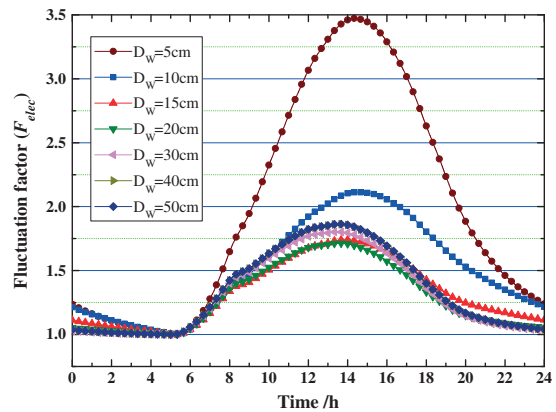


Figure 7. The influence of water layer depth on fluctuation factor.

power, accompanied by a drop of the output power peak value. When the depth of water energy storage layer is less than 20 cm, it could be heated more effectively by the sandstone surface as the water layer depth decreases, thus the daytime output power peak value decreases with increasing water layer depth. During the night, due to the same varying trend in depth and energy storage capability of water layer as well as system output power valley value, the output power fluctuation factor changes insignificantly along with the increase of water layer depth. However, when the depth is above 20 cm, both the output power peak and valley values fall along with an increasing water layer depth. The phenomenon can be explained as follows: with a thin water layer, the water temperature is higher and the heat transmission to the air faster at night, and with a thick water layer, the overall water temperature is lower, and the temperature difference with the air is not big enough for rapid transfer. Consequently, an optimum value for water layer depth should be found when applying the hybrid energy storage system. According to the calculating model of the 100 MW level solar chimney power generating system and corresponding energy storage materials, the optimum water depth is 5 cm as the total generating capacity

Table III. The influence of the water layer depth on system performance.

Water depth	P [GWh/day]	$P_{elec, max}$ [MW]	$P_{elec, min}$ [MW]	F_{elec}
$D_w = 0$ cm	1.41	123.29	19.19	6.42
$D_w = 5$ cm	1.52	108.95	31.38	3.47
$D_w = 10$ cm	1.47	85.12	40.29	2.11
$D_w = 15$ cm	1.49	80.85	46.43	1.74
$D_w = 20$ cm	1.45	79.89	46.63	1.71
$D_w = 30$ cm	1.39	78.75	43.69	1.80
$D_w = 40$ cm	1.33	76.28	41.00	1.86
$D_w = 50$ cm	1.28	73.84	38.80	1.90

reaches its peak within a day and 20 cm as the fluctuation factor peak value arrives at its bottom.

Furthermore, there is an interesting phenomenon worth mentioning, that is, as the water layer depth changes, the occurrence time of output power peak value and fluctuation factor undergoes a reverse changing trend with time. When the water depth is within 10 cm, its increase will result in a later occurrence of the output power and fluctuation factor peak values, whereas they would appear in advance when it is beyond 10 cm and will remain stable without significant change despite of increasing depth. This phenomenon can also be seen if we go through the simulation results shown by Bernardes in 2003 [9]. However, there is no further explanation for this phenomenon in reference [9]. The authors hold the view that it may be related to the energy storage features of the water and the sandstone layer below. Though solar radiation has already reached the maximum after 12 o'clock and decreases gradually (but ambient temperature increases slightly till 15 h in Table II), thanks to thin water layer, both the water and the sandstone of the energy storage layer could continue to raise their temperatures. Then they both could supply the air inside the collector with an increasing amount of thermal energy, which results in an increase of output power, thus leading to a delay of peak value of output power occurrence. Reversely, if the water layer is thick enough, the energy absorbed by the sandstone energy storage layer below deep water would be impossible to be transferred to the air upside but would gradually be stored down deeper into the ground. Therefore, when solar radiation begins to decrease, the storage system is unable to provide more energy for air inside the collector aiming at creating system driving force, thus resulting in an earlier maximum occurrence.

The phenomenon of reverse changing trend of peak values along with time would be helpful in effective prediction of optimum water depth. For an SC system with hybrid energy storage layer made of water and sandstone, both output power and fluctuation factor would approach their optimum values when the phenomenon of reverse variation trend of peak values along with time occurred. In the meantime, it is useless to increase the water depth. The simulation results shown in Table III are in accordance with the analysis above.

5.3. Influence of water layer area on SC performances

The influence of water area on SC performances will be explored by using a hybrid energy storage system model. In the calculation, the water layer is assumed to be 10 cm in depth, and A_w , being defined as the ratio between the area of water layer and the total area of the energy storage layer, is considered as 25%, 50%, 75% and 100%, respectively. The water layer is placed from outside to inside, for example, $A_w = 25\%$ means that a water layer of 10 cm in depth constitutes 25% of the total area of the external side of the storage layer and 75% of the internal side is covered by sandstone materials. Figure 8 shows the effect of water-energy storage area on output power, with $A_w = 0\%$ representing a layout which solely employs sandstone for energy storing. Figure 9 is the influence of the area of water layer on system fluctuation factor. It is obvious that along with the increase of water layer area, the peak value of output power decreases significantly while the valley value changes reversely, thus resulting in a more stable system with less power generation fluctuation.

5.4. Influence of water layer location on SC performances

Adopting the hybrid energy storage system, we will explore the influence of water layer location on system

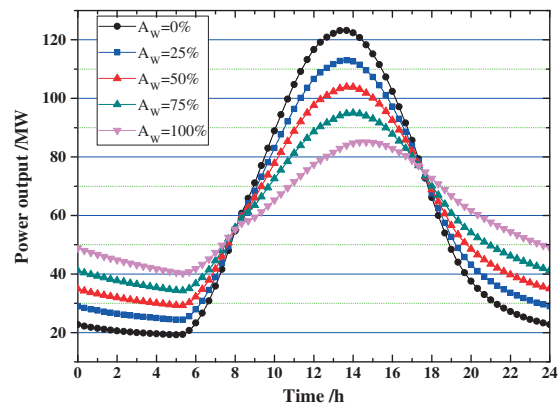


Figure 8. The influence of water energy storage area on output power.

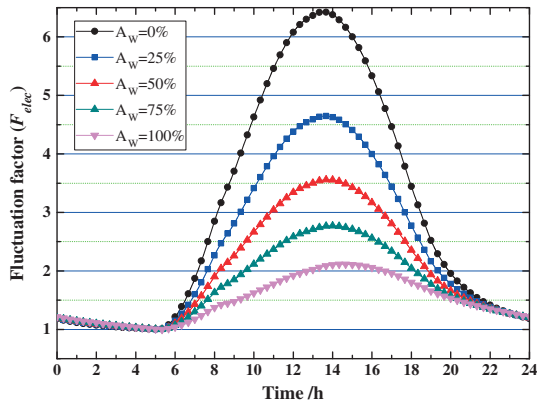


Figure 9. The influence of water energy storage layer area on system fluctuation factor.

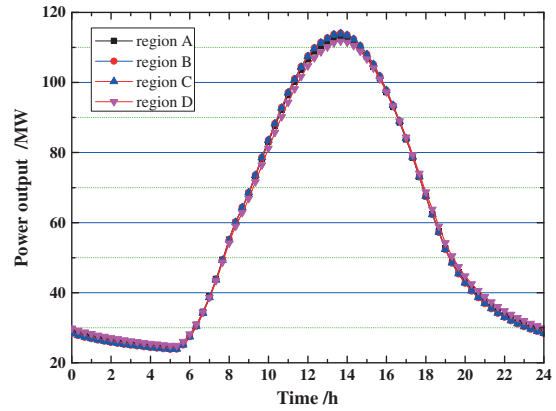


Figure 12. The influence of location of water energy storage layer on system output power.

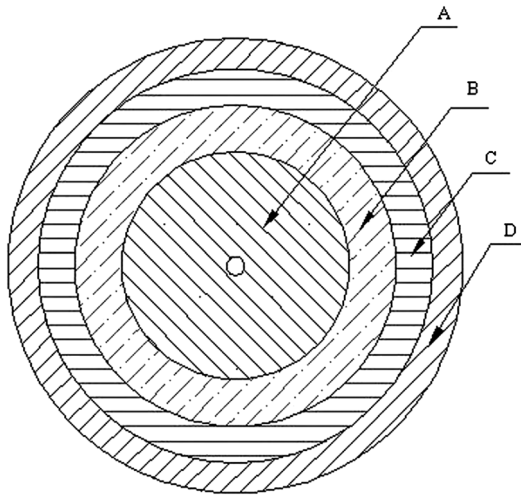


Figure 10. Sketch of the location of water energy storage layer.

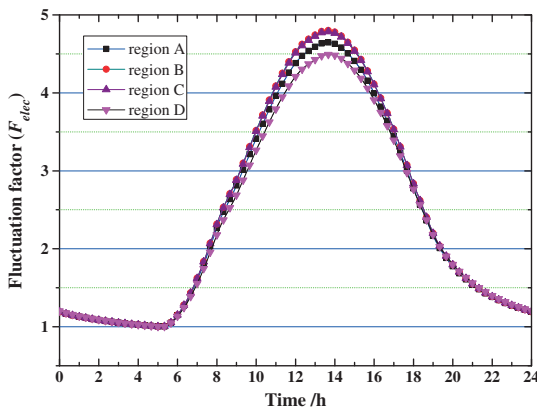


Figure 11. The influence of location of water energy storage layer on system fluctuation factor.

performances. In the calculation, four regions with the same area as shown in Figure 10 are taken into consideration for the disposal of water layer, the water depth and A_w being assumed as 10 cm and 25%, respectively. Figures 11, 12 show that the fluctuation factor and output power curves along with time of regions A, B and C almost superpose while the fluctuation factor of D is relatively smaller. However, in general, with certain depth and area of the water layer, the location would only exert slight influence on system output power and fluctuation factor.

6. CONCLUSION

With the intention of finding out a smoothing method for the fluctuation and intermittence features of SC systems, and to smooth the peak-to-valley of the output power, the approach of adopting a hybrid energy storage system of water and sandstone is proposed. Different energy storage models are employed to serve the calculation of a 100 MW SC system. The results indicate that the water energy storage layer could notably reduce the difference between peak and valley values of system output power as well as efficiently diminish the system fluctuation factor. Furthermore, the optimum depth of the water layer could be predicted by the reverse changing trend of peak values along with time of the system output power and fluctuation factor, and the location of the water layer would only exert slight influence upon fluctuation factor.

NOMENCLATURE

Latin symbols

- A = areas [m^2]
- c = specific heat [$J \cdot kg^{-1} \cdot K^{-1}$]
- f = fanning friction factor [-]

F	= fluctuation factor
g	= gravitational acceleration, $9.8 \text{ [m}\cdot\text{s}^{-2}]$
H	= height [m]
h	= heat transfer convection coefficient $[\text{W}\cdot\text{m}^{-2}\cdot\text{K}^{-1}]$
h_r	= radiation heat transfer coefficient $[\text{W}\cdot\text{m}^{-2}\cdot\text{K}^{-1}]$
L	= length of collector [m]
\dot{m}	= mass flow rate $[\text{kg}\cdot\text{s}^{-1}]$
Nu	= Nusselt number [-]
P	= power or pressure $[\text{W}]/[\text{N}\cdot\text{m}^{-2}]$
Pe	= perimeter [m]
Pr	= Prandtl number [-]
r	= radius [m]
Re	= Reynolds number [-]
R_l	= ideal gas constant, $287.05 \text{ [J}\cdot\text{kg}^{-1}\cdot\text{K}^{-1}]$
S	= absorbed solar radiation $[\text{W}\cdot\text{m}^{-2}]$
S_{sun}	= incident solar radiation $[\text{W}\cdot\text{m}^{-2}]$
T	= temperature [K]
u	= velocity $[\text{m}\cdot\text{s}^{-1}]$
x	= factor of pressure drop at the turbine [-]
y	= thickness [m]

Greek symbols

α	= extinction coefficient
β	= absorptivity
ε	= emissivity
σ	= Stefan-Boltzmann constant, $5.67 \times 10^{-8} \text{ [W}\cdot\text{m}^{-2}\cdot\text{K}^{-4}]$
λ	= thermal conductivity $[\text{W}\cdot\text{m}^{-1}\cdot\text{K}^{-1}]$
η	= efficiency
Δ	= differential
τ	= time [s]
ρ	= density $[\text{kg}\cdot\text{m}^{-3}]$

Subscripts

a	= ambient
avg	= average
c	= chimney
$coll$	= collector
dyn	= dynamic
$elec$	= electricity
f	= airflow
g	= ground/generator
gf	= ground to air under collector roof
i	= Inlet
o	= outlet
p	= constant pressure
ra	= collector to ambient air
rf	= collector roof
s	= storage
tot	= total
$turb$	= turbine

ACKNOWLEDGEMENTS

This research was supported by the National Natural Science Foundation of China (51106060), the China Postdoctoral Science Foundation Fourth Special Funded Project (201104460) and the HUST Innovative Foundation (2011TS076).

REFERENCES

1. Haaf W, Friedrich K, Mayr G, Schlaich J. Solar chimneys, part I: principle and construction of the pilot plant in Manzanares. *International Journal of Solar Energy* 1983; **2**:3–20.
2. Haaf W. Solar chimneys, part II: preliminary test results from the Manzanares pilot plant. *International Journal of Solar Energy* 1984; **2**:141–161.
3. Yan MQ, Sherif SA, Kridli GT, Lee SS, Padki MM. Thermo-fluids analysis of solar chimneys. *Industrial Application of Fluid Mechanics* 1991; **ASME FED-2**:125–30.
4. Pasumarthi N, Sherif SA. Experimental and theoretical performance of a demonstration solar chimney model-part I: mathematical model development. *International Journal of Energy Research* 1998; **22**:277–288.
5. Pasumarthi N, Sherif SA. Experimental and theoretical performance of a demonstration solar chimney model-part II: experimental and theoretical results and economic analysis. *International Journal of Energy Research* 1998; **22**(5):443–461.
6. Padki MM, Sherif SA. On a simple analytical model for solar chimneys. *International Journal of Energy Research* 1999; **23**(4):345–349.
7. Gannon AJ, von Backström TW. Solar chimney cycle analysis with system loss and solar collector performance. *Journal of Solar Energy Engineering, Transaction of ASME* 2000; **122**:133–137.
8. Gannon AJ, von Backström TW. Solar chimney turbine performance. *Journal of Solar Energy Engineering, Transaction of ASME* 2003; **125**:101–106.
9. Bernardes MADS, Vob A, Weinrebe G. Thermal and technical analyses of solar chimneys. *Solar Energy* 2003; **75**:511–524.
10. von Backström TW, Fluri TP. Maximum fluid power condition in solar chimney power plants—an analytical approach. *Solar Energy* 2006; **80**(11):1417–1423.
11. Pretorius JP, Kröger DG. Solar chimney power plant performance. *Journal of Solar Energy Engineering, Transaction of ASME* 2006; **128**:302–311.
12. Pretorius JP, Kröger DG. Critical evaluation of solar chimney power plant performance. *Solar Energy* 2006; **80**:535–544.

13. Ming TZ, Liu W, Xu GL. Analytical and numerical simulation of the solar chimney power plant systems. *International Journal of Energy Research* 2006; **30**(11):861–873.
14. Ming TZ, Zheng Y, Liu C, *et al.* Simple analysis on thermal performance of solar chimney power generation systems. *Journal of the Energy Institute* 2010; **83**(1):6–11.
15. Zheng Y, Ming TZ, Zhou Z, *et al.* Unsteady numerical simulation of solar chimney power plant system with energy storage layer. *Journal of the Energy Institute* 2010; **83**(2):86–92.
16. Bernardes MADS, von Backström TW, Kröger DG. Analysis of some available heat transfer coefficients applicable to solar chimney power plant collectors. *Solar Energy* 2009; **83**:264–275.
17. Bernardes MADS, von Backström TW. Evaluation of operational control strategies applicable to solar chimney power plants. *Solar Energy* 2010; **84**:277–288.
18. Nizetic S, Ninic N, Klarin B. Analysis and feasibility of implementing solar chimney power plants in the Mediterranean region. *Energy* 2008; **33**:1680–1690.
19. Maia CB, Ferreira AG, Valle RM, Cortez MFB. Theoretical evaluation of the influence of geometric parameters and materials on the behavior of the airflow in a solar chimney. *Computers & Fluids* 2009; **38**:625–636.
20. Maia CB, Ferreira AG, Valle RM, Cortez MFB. Analysis of the Airflow in a Prototype of a Solar Chimney Dryer. *Heat Transfer Engineering* 2009; **30**:393–399.
21. Ferreira AG, Maia CB, Cortez MFB, Valle RM. Technical feasibility assessment of a solar chimney for food drying. *Solar Energy* 2008; **82**:198–205.
22. Nizetic S, Klarin B. A simplified analytical approach for evaluation of the optimal ratio of pressure drop across the turbine in solar chimney power plants. *Applied Energy* 2010; **87**:587–591.
23. Ming TZ, Wang XJ, de Richter RK, Liu W, Wu TH, Pan Y. Numerical analysis on the influence of ambient crosswind on the performance of solar updraft power plant system. *Renewable and Sustainable Energy Reviews* 2012; **16**:5567–5583.
24. Kirstein CF, von Backström TW. Flow through a solar chimney power plant collector-to-chimney transition section. *Journal of Solar Energy Engineering* 2006; **128**(3):312–317.
25. Ming TZ, de Richter RK, Meng FL, *et al.* Chimney shape numerical study for solar chimney power generating systems. *International Journal of Energy Research* 2011. Available at: <http://onlinelibrary.wiley.com/doi/10.1002/er.1910/full>
26. Busch D, Harte R, Krätzig WB, Montag U. New Natural Draft Cooling Tower of 200 m of height. *Engineering Structures* 2002; **24**(12):1509–1521.
27. Krätzig WB, Harte R, Montag U, Wörmann R. From large natural draft cooling tower shells to chimneys of solar updraft power plants. *Proceedings of the International Association for Shell and Spatial Structures (IASS)*, 2009, Valencia, Spain.
28. Harte R, Krätzig WB, Niemann HJ. From Cooling Towers to Chimneys of Solar Upwind Power Plants. 10p in *Proceedings of 2009 Structures Congress*, Austin, Texas.
29. Kreetz H. Theoretische Untersuchungen und Auslegung eines temporären Wasserspeichers für das Aufwindkraftwerk. diploma thesis, Technical University Berlin, Berlin, 1997.
30. Ming TZ, Liu W, Pan Y, Xu GL. Numerical analysis of flow and heat transfer characteristics in solar chimney power plants with energy storage layer. *Energy Conversion and Management* 2008; **49**:2872–2879.
31. Xu GL, Ming TZ, Pan Y, Meng FL, Zhou C. Numerical analysis on the performance of solar chimney power plant system. *Energy Conversion and Management* 2011; **52**:876–883.
32. Holman JP. *Heat Transfer*. (9th edn.), McGraw Hill: New York, 2006.
33. http://en.wikipedia.org/wiki/Adiabatic_process
34. http://mintaka.sdsu.edu/GF/explain/thermal/std_atm.html
35. Kundu PK, Cohen IM. *Fluid Mechanics*. (2nd edn.) Academic Press: San Diego, 2002.